Journal Name

ARTICLE TYPE

Cite this: DOI: 10.1039/xxxxxxxxxx

A complex-polarization-propagator protocol for magneto-chiral axial dichroism and birefringence dispersion†

Janusz Cukras,[ab] Joanna Kauczor,[c] Patrick Norman,[c] Antonio Rizzo,[d] Geert L.J.A. Rikken,[e] and Sonia Coriani*[af]

Received Date
Accepted Date

DOI: 10.1039/xxxxxxxxxx

www.rsc.org/journalname

A computational protocol to magneto-chiral dichroism and magneto-chiral birefringence dispersion is presented within the framework of damped response theory, also known as complex polarization propagator theory, at the level of time-dependent Hartree–Fock and time-dependent density functional theory. Magneto-chiral dichroism and magneto-chiral birefringence spectra in the (resonant) frequency region below the first ionization threshold of R-methyloxirane and L-alanine are presented and compared with corresponding results for both the electronic circular dichroism and the magnetic circular dichroism. The additional information content yielded by the magneto-chiral phenomena, as well as their potential experimental detectability for the selected species are discussed.

1 Introduction

Magneto-chiral dichroism (MChD) [1–10] is related to the difference in the absorption coefficients of a chiral molecule in a magnetic field parallel and antiparallel to the incident light beam. In other words, if one shines light (in any polarization state) on a chiral species in presence of a static magnetic field with a component parallel to the direction of propagation of the light, the absorption coefficient $n'^{\uparrow\uparrow}$ for **B** (magnetic field) and **k** (direction of propagation) parallel to each other differs from the one measured for **B** and **k** antiparallel, $n'^{\uparrow\downarrow}$. The same occurs for the refractive indices, and the resulting birefringence, corresponding to an anisotropy of the phase of the beams, is then known as magneto-chiral birefringence (MChB). [1–9,11] The two effects will moreover be oppositely signed for the two mirror-image enantiomers, or reversing the relative directions of the magnetic field and the propagation vector.

Magneto-chiral dichroism has long been considered a plausible candidate for explaining the homochirality of life, in addition to the Earth's rotational motion and circularly polarized light induced asymmetric photochemical reactions. [5,7,12] Yet, its experimental detection in compounds of relevance in life sciences, like aminoacids, is elusive. The only experimental reports of MChD spectra of organic molecules concern a porphyrin complex [13] and an artificial light-harvesting antenna. [14] Recently, a report appeared on the detection of strong magneto-chiral dichroism in a paramagnetic molecular helix observed by hard X-rays. [15]

This is clearly a case where computational simulations can be of fundamental help. However, no computational protocol for MChD has been proposed so far, despite the fact that a molecular theory of the effect has been available for more than thirty years, [4] and it bears strong similarities with the theory of magnetic circular dichroism (MCD). [16–18]

Building upon our expertise on the development of computational methods for magnetic circular dichroism, [19–23] and magneto-chiral birefringence, [24,25] we present here the definition and implementation of a computational protocol for magneto-chiral dichroism and birefringence dispersion in the framework of the complex polarization propagation approach (CPP), also known as damped response theory. [26–30] In the CPP approach, an empirical line width parameter is introduced in the response functions to account for the finite lifetime of the excited states. The real and imaginary components of the resulting complex response function are well-behaved even in the resonant regions of the spectrum. Depending on the perturbation operators involved, dispersion and absorption contributions to a given physical phenomenon are identified by the real and imaginary components.

[a]*Dipartimento di Scienze Chimiche e Farmaceutiche, Università degli Studi di Trieste, via Giorgieri 1, 34127 Trieste, Italy*
[b]*Faculty of Chemistry, University of Warsaw, Pasteura 1, 02-093 Warszawa, Poland.*
[c]*Department of Physics, Chemistry and Biology, Linköping University, S-58183, Linköping, Sweden*
[d]*Consiglio Nazionale delle Ricerche - CNR, Istituto per i Processi Chimico-Fisici, Sede Secondaria di Pisa, Area della Ricerca, Via G. Moruzzi 1, I-56124 Pisa, Italy*
[e]*Laboratoire National des Champs Magnétiques Intenses, UPR3228 CNRS/INSA/UJF/UPS, Toulouse & Grenoble, France.*
[f]*Aarhus Institute of Advanced Studies, Aarhus University, DK-8000 Aarhus C, Denmark*
*Corresponding author. E-mail: coriani@units.it
† Electronic Supplementary Information (ESI) available: [details of any supplementary information available should be included here]. See DOI: 10.1039/b000000x/

These are almost straightforwardly identified with the molecular property tensors emerging within the semi-classical formalism when considering the oscillating electric and magnetic multipole moments induced by the incident light wave.[1,31] Thus, for instance, the imaginary part of the electric dipole–electric dipole linear response function relates to the one-photon absorption spectrum;[26] the real part of the electric dipole–magnetic dipole linear response function yields the electronic circular dichroism (ECD) spectrum;[32] the real part of the electric dipole–electric dipole–magnetic dipole quadratic response function connects to the MCD spectrum; its imaginary counterpart gives the dispersion of the Faraday rotation (angle).[21]

Our ultimate purpose is to use the proposed protocol to estimate the effect on molecular systems important in life sciences, in an attempt to identify which compounds may have a response above the detectability limit of the current experimental setups. Here, we will present pilot results for R-methyloxirane and L-alanine.

2 Theory

The expression of the molecular quantities describing magneto-chiral birefringence (MChB) and magneto-chiral dichroism (MChD) can be derived either within the refractive index approach or within the rifrangent scattering approach, similarly as for one-photon absorption (OPA), optical rotation dispersion (ORD) and electronic circular dichroism (ECD), magnetic optical rotatory dispersion (MORD) and magnetic circular dichroism (MCD). Both approaches have been extensively discussed in the literature, see e.g. Buckingham[31] and Barron.[1] Here we follow closely Ref. 4.

Within the refractive index approach, the refractive and absorption indices of incident light of circular frequency ω passing through a diluted molecular medium of number density N are expressed in terms of appropriate combinations of dynamical molecular tensors. For light linearly polarized along x and propagating in the z direction we have, for the refraction (n) and absorption (n') indices, respectively

$$n \approx 1 + \frac{N}{4\varepsilon_0}[\alpha_{xx}(f) + \zeta_{xxz}(f)\cdots] \tag{1}$$

$$n' \approx \frac{N}{4\varepsilon_0}[\alpha_{xx}(g) + \zeta_{xxz}(g)\cdots] \tag{2}$$

Above ε_0 is the electric constant. The molecular tensors on the right-hand side of the above expressions are components of the complex dynamic dipole polarizability tensor (Barron's notation[1]) $\tilde{\alpha}_{\alpha\beta} = \alpha_{\alpha\beta} - i\alpha'_{\alpha\beta}$ and of the optical rotatory tensor

$$\tilde{\zeta}_{\alpha\beta\lambda} = \zeta_{\alpha\beta\lambda} - i\zeta'_{\alpha\beta\lambda} \tag{3}$$

$$\zeta_{\alpha\beta\lambda} = \frac{1}{c_0}\left[\frac{1}{3}\omega(A'_{\alpha,\beta\lambda} + A'_{\beta,\alpha\lambda}) + \varepsilon_{\delta\lambda\alpha}G_{\beta\delta} + \varepsilon_{\delta\lambda\beta}G_{\alpha\delta}\right] \tag{4}$$

$$\zeta'_{\alpha\beta\lambda} = -\frac{1}{c_0}\left[\frac{1}{3}\omega(A_{\alpha,\beta\lambda} - A_{\beta,\alpha\lambda}) + \varepsilon_{\delta\lambda\alpha}G'_{\beta\delta} - \varepsilon_{\delta\lambda\beta}G'_{\alpha\delta}\right] \tag{5}$$

where c_0 is the speed of light in vacuo, and $\varepsilon_{\alpha\beta\lambda}$ is the alternating (Levi-Civita) tensor. Each molecular tensor is further decomposed in dispersive (i.e. a dispersion line-shape function is associated with the tensor) and absorptive components, as indicated by the (f) and (g) notation, respectively. For instance,

$$\alpha_{\alpha\beta} = \alpha_{\alpha\beta}(f) + i\alpha_{\alpha\beta}(g)\ . \tag{6}$$

Explicit sum-over-states expressions for the electric dipole–magnetic dipole ($\tilde{G}_{\alpha\beta} = G_{\alpha\beta} - iG'_{\alpha\beta}$) and electric dipole–electric quadrupole ($\tilde{A}_{\alpha,\beta\gamma} = A_{\alpha,\beta\gamma} - iA'_{\alpha,\beta\gamma}$) dynamic molecular tensors can be found e.g. in Refs. 1,31, see also Ref. 4.

For circularly polarized light the equations are[4]

$$n^{R/L} \approx 1 + \frac{N}{4\varepsilon_0}\{\alpha_{xx}(f) + \alpha_{yy}(f) + \zeta_{xxz}(f) + \zeta_{yyz}(f) \mp 2[\alpha'_{xy}(f) + \zeta'_{xyz}(f)] + \cdots\}\ , \tag{7}$$

$$n'^{R/L} \approx \frac{N}{4\varepsilon_0}\{\alpha_{xx}(g) + \alpha_{yy}(g) + \zeta_{xxz}(g) + \zeta_{yyz}(g) \mp 2[\alpha'_{xy}(g) + \zeta'_{xyz}(g)] + \cdots\} \tag{8}$$

where superscripts R and L indicate right and left circular polarization, respectively. For unpolarized light (regarded as incoherent superposition of right and left circularly polarized light) we have[4]

$$n \approx 1 + \frac{N}{4\varepsilon_0}[\alpha_{xx}(f) + \alpha_{yy}(f) + \zeta_{xxz}(f) + \zeta_{yyz}(f)] \tag{9}$$

$$n' \approx \frac{N}{4\varepsilon_0}[\alpha_{xx}(g) + \alpha_{yy}(g) + \zeta_{xxz}(g) + \zeta_{yyz}(g)] \tag{10}$$

The quantities $\alpha_{xx}(g) + \alpha_{yy}(g)$ and $\zeta_{xxz}(g) + \zeta_{yyz}(g)$, are independent of the polarization state of incident light and, while canceling out for natural optical activity, they are responsible for conventional absorption and for magneto-chiral dichroism, respectively. The polarization-dependent terms $\alpha_{xx}(g) - \alpha_{yy}(g)$ and $\alpha_{xy}(g)$ are responsible for linear dichroism, $\zeta_{xxz}(g) - \zeta_{yyz}(g)$ and $\zeta_{xyz}(g)$ for gyrotropic dichroism, $\alpha'_{xy}(g)$ for magnetic circular dichroism, and $\zeta'_{xyz}(g)$ for natural circular dichroism.[1,4]

When a static magnetic field **B** aligned with the direction of propagation z is applied to the diluted medium, within a perturbative approach including only terms linear in B_z, the electric dipole polarizability $\tilde{\alpha}_{\alpha\beta}$ and the molecular tensors entering Eqs. 4 and 5 are modified as follows

$$\alpha_{\alpha\beta}(B_z) = \alpha_{\alpha\beta} + \alpha^{(m)}_{\alpha\beta,z}B_z \tag{11}$$

$$\alpha'_{\alpha\beta}(B_z) = \alpha'_{\alpha\beta} + \alpha'^{(m)}_{\alpha\beta,z}B_z \tag{12}$$

$$A'_{\alpha,\beta\lambda}(B_z) = A'_{\alpha,\beta\lambda} + A'^{(m)}_{\alpha,\beta\lambda,z}B_z \tag{13}$$

$$G_{\alpha\beta}(B_z) = G_{\alpha\beta} + G^{(m)}_{\alpha\beta,z}B_z \tag{14}$$

MChB and MChD anisotropies arise when the effect of the static perturbing magnetic field is included in the expressions of the refractive indices for unpolarized light (Eqs. 9–10, and similarly for linearly polarized light) for two different reciprocal orientations

(parallel, $\uparrow\uparrow$, and antiparallel $\uparrow\downarrow$) of the direction of propagation and of the external magnetic field. A classical Boltzmann average over all orientations taken by the molecules of the medium in a fluid yields then the following expressions

$$n^{\uparrow\uparrow} - n^{\uparrow\downarrow} \approx \frac{N}{3\varepsilon_0 c_0} B_z \left\{ \frac{\omega}{15} [3A'^{(m)}_{\alpha,\alpha\beta,\beta}(f) - A'^{(m)}_{\alpha,\beta\beta,\alpha}(f)] + \varepsilon_{\alpha\beta\lambda} G^{(m)}_{\alpha\beta,\lambda}(f) \right\}$$

$$\equiv \frac{N}{3\varepsilon_0 c_0} B_z \left\{ B^{A'}(f) + B^{G}(f) \right\} \quad (15)$$

$$n'^{\uparrow\uparrow} - n'^{\uparrow\downarrow} \approx \frac{N}{3\varepsilon_0 c_0} B_z \left\{ \frac{\omega}{15} [3A'^{(m)}_{\alpha,\alpha\beta,\beta}(g) - A'^{(m)}_{\alpha,\beta\beta,\alpha}(g)] + \varepsilon_{\alpha\beta\lambda} G^{(m)}_{\alpha\beta,\lambda}(g) \right\}$$

$$\equiv \frac{N}{3\varepsilon_0 c_0} B_z \left\{ B^{A'}(g) + B^{G}(g) \right\} \quad (16)$$

Before proceeding we give here some relevant definitions and establish the notation used later when comparing our results for MChD and MChB with other closely related dichroisms and birefringences. In conventional OPA, the quantity of interest is the absorption coefficient n' for unpolarized light, and the molecular tensor quantity responsible for it is then $\alpha_{xx}(g) + \alpha_{yy}(g)$. For a sample of randomly oriented (achiral) molecules, in absence of external magnetic fields, tumble-averaging yields

$$n' \approx \frac{N}{6\varepsilon_0} \alpha_{\alpha\alpha}(g) \quad (17)$$

In the following we will report the OPA spectra as absorption cross section σ in au (the SI unit is the barn = 10^{-28} m^2)

$$\sigma(\omega) = \frac{\omega}{3\varepsilon_0 c_0} \alpha_{\alpha\alpha}(g) \quad (18)$$

$$\sigma(\omega)[\text{au}] \approx 3.05671 \times 10^{-2} \times \omega[\text{au}] \alpha_{\alpha\alpha}(g)[\text{au}] \quad (19)$$

$$\sigma(\omega)[\text{barn}] \approx 8.55965 \times 10^{5} \times \omega[\text{au}] \alpha_{\alpha\alpha}(g)[\text{au}] \quad (20)$$

The last two equations yield the observable in atomic units and SI, respectively, when the circular frequency ω and the molecular tensor $\alpha_{\alpha\alpha}(g)$ are given in atomic units.

For circularly differential refractive effects, as those yielding natural optical activity (NOA) and magnetic-field-induced optical activity (MOA), we deal with an anisotropy of the refractive and the absorptive indices for light polarized in the L and R directions. This yields specifically a rotation $\Delta\theta$ or an ellipticity η, in radians, which can (always) be written as (l is the optical path length) [1]

$$\Delta\theta = \frac{\omega l}{2c_0}(n^L - n^R); \quad (21)$$

$$\eta = \frac{\omega l}{2c_0}(n'^L - n'^R) \quad (22)$$

In experiments, the quantities of relevance are the *specific* or the *molar* rotations ($[\alpha]$ and $[\phi]$, respectively) and ellipticities ($[\psi]$ and $[\Theta]$, respectively), defined as optical rotations (ellipticities) per unit path length (given in decimeter for specific observables and in centimeter for molar quantities) divided by the density d of the sample (given in grams per liter for the specific observables and in 10^{-2} moles per liter for molar quantities). Equations for specific properties are given in the Appendix. Here we report explicit expression for molar quantities.

In NOA the polarization-dependent $\zeta'_{xyz}(f)$ and $\zeta'_{xyz}(g)$ tensors are of relevance. Tumble averaging further reduces the anisotropies to the contribution from the $G'_{\alpha\beta}$ tensor alone

$$\Delta n \approx -\frac{2N}{3\varepsilon_0 c_0} G'_{\alpha\alpha}(f) \quad (23)$$

$$\Delta n' \approx -\frac{2N}{3\varepsilon_0 c_0} G'_{\alpha\alpha}(g) \quad (24)$$

In terms of molar observables

$$[\phi]^{\text{OR}} \approx -\frac{100\ \omega N_a}{3\varepsilon_0 c_0^2} G'_{\alpha\alpha}(f) \quad (25)$$

$$[\Theta]^{\text{ECD}} \approx -\frac{100\ \omega N_a}{3\varepsilon_0 c_0^2} G'_{\alpha\alpha}(g) = -\frac{100\ \text{Ln}(10)}{4} \Delta\varepsilon' \quad (26)$$

In the last equation we introduced the molar absorptivity ε' (SI units of m^3 mol^{-1}; usual units cm^{-1} mol^{-1} dm^3). N_a is Avogadro's constant. The molar rotation (ellipticity) is obtained in the commonly used units of deg $\times$ dm^3 $\times$ cm^{-1} $\times$ mol^{-1} via the expressions (the conversion from radians to degrees implies the multiplication by the factor $180/\pi$)

$$[\phi]^{\text{OR}}[\text{deg} \times \text{dm}^3 \times \text{cm}^{-1} \times \text{mol}^{-1}] \approx \quad (27)$$

$$-2.15524 \times 10^4 \times \omega[\text{au}] \times G'_{\alpha\alpha}(f)[\text{au}]$$

$$[\Theta]^{\text{ECD}}[\text{deg} \times \text{dm}^3 \times \text{cm}^{-1} \times \text{mol}^{-1}] \approx \quad (28)$$

$$-2.15524 \times 10^4 \times \omega[\text{au}] \times G'_{\alpha\alpha}(g)[\text{au}]$$

$$[\Theta]^{\text{ECD}}[\text{deg} \times \text{dm}^3 \times \text{cm}^{-1} \times \text{mol}^{-1}] \approx \quad (29)$$

$$-3.29821 \times 10^3 \times \Delta\varepsilon'[\text{cm}^{-1}\text{mol}^{-1}\text{dm}^3]$$

where, as for Eqs. 20 and 19 above and in other instances below, we specify within square brackets the units to be employed for the quantities in the right hand side to obtain the observable in the units given in the left side of the Equations.

In MORD and MCD, manifestations of MOA, the effect of a static magnetic field on the tensors entering the indices for the RCP and LCP components of plane-polarized light (again Eqs. 7-8) to first order in the magnetic field is considered. Only the first-order response $\alpha'^{(m)}_{\alpha\beta\lambda}$ of the antisymmetric polarizability $\alpha'_{\alpha\beta}$, see Eq. 12, survives, yielding a non vanishing contribution to the anisotropies. After averaging, we obtain

$$\Delta n = -\frac{N}{6\varepsilon_0} B_z \varepsilon_{\alpha\beta\lambda} \alpha'^{(m)}_{\alpha\beta\lambda}(f) \quad (30)$$

$$\Delta n' = -\frac{N}{6\varepsilon_0} B_z \varepsilon_{\alpha\beta\lambda} \alpha'^{(m)}_{\alpha\beta\lambda}(g) \quad (31)$$

In terms of molar observables

$$[\phi]^{\mathrm{MOR}} \approx -\frac{25\omega N_a}{3\varepsilon_0 c_0} B_z \varepsilon_{\alpha\beta\lambda} \alpha'^{(m)}_{\alpha\beta\lambda}(f) \tag{32}$$

$$[\Theta]^{\mathrm{MCD}} \approx -\frac{25\omega N_a}{3\varepsilon_0 c_0} B_z \varepsilon_{\alpha\beta\lambda} \alpha'^{(m)}_{\alpha\beta\lambda}(g) \tag{33}$$

$$[\phi]^{\mathrm{MOR}}[\mathrm{deg}\times\mathrm{dm}^3\times\mathrm{cm}^{-1}\times\mathrm{mol}^{-1}] \approx$$

$$-3.14128\times\omega[\mathrm{au}]\times B_z[\mathrm{T}]\times\varepsilon_{\alpha\beta\lambda}\times\alpha'^{(m)}_{\alpha\beta\lambda}(f)[\mathrm{au}] \tag{34}$$

$$[\Theta]^{\mathrm{MCD}}[\mathrm{deg}\times\mathrm{dm}^3\times\mathrm{cm}^{-1}\times\mathrm{mol}^{-1}] \approx$$

$$-3.14128\times\omega[\mathrm{au}]\times B_z[\mathrm{T}]\times\varepsilon_{\alpha\beta\lambda}\times\alpha'^{(m)}_{\alpha\beta\lambda}(g)[\mathrm{au}] \tag{35}$$

Although the MChB and MChD are not circular differential properties, for the sake of comparing quantities with the same units we generalize Eqs. 21 and 22 to axial anisotropies and define molar observables as

$$[\phi]^{\mathrm{MChB}} = \frac{\omega l}{2c_0}(n^{\uparrow\uparrow} - n^{\uparrow\downarrow}) \approx \frac{50\omega N_a}{3\varepsilon_0 c_0^2} B_z \left\{ B^{A'}(f) + B^G(f) \right\} \tag{36}$$

$$[\Theta]^{\mathrm{MChD}} = \frac{\omega l}{2c_0}(n'^{\uparrow\uparrow} - n'^{\uparrow\downarrow}) \approx \frac{50\omega N_a}{3\varepsilon_0 c_0^2} B_z \left\{ B^{A'}(g) + B^G(g) \right\} \tag{37}$$

$$[\phi]^{\mathrm{MChB}}[\mathrm{deg}\times\mathrm{dm}^3\times\mathrm{cm}^{-1}\times\mathrm{mol}^{-1}] \tag{38}$$

$$\approx 4.58460\times10^{-2}\times\omega[\mathrm{au}]\times B_z[\mathrm{T}]\times\left\{ B^{A'}(f) + B^G(f) \right\}[\mathrm{au}]$$

$$[\Theta]^{\mathrm{MChD}}[\mathrm{deg}\times\mathrm{dm}^3\times\mathrm{cm}^{-1}\times\mathrm{mol}^{-1}] \tag{39}$$

$$\approx 4.58460\times10^{-2}\times\omega[\mathrm{au}]\times B_z[\mathrm{T}]\times\left\{ B^{A'}(g) + B^G(g) \right\}[\mathrm{au}]$$

Note that temperature-dependent terms have been omitted in the expressions above, since they involve the expectation-value of the magnetic dipole operator in the ground state, which is quenched for closed shell systems as those we consider in this study.

A criterion to decide on whether or not magneto-chiral dichroism in a particular absorption band is measurable for a given instrumental sensitivity is given by the so-called magneto-chiral dissymmetry (or asymmetry) factor g_{MChA} or g_{MChD} (also known as δ),[4,7]

$$g_{\mathrm{MChD}}(B) = \frac{n'^{\uparrow\uparrow} - n'^{\uparrow\downarrow}}{\frac{1}{2}(n'^{\uparrow\uparrow} + n'^{\uparrow\downarrow})} = 2\frac{B_z[B^{A'}(g) + B^G(g)]}{c_0 \cdot \alpha_{\alpha\alpha}(g)} \tag{40}$$

The denominator in the magneto-chiral dissymmetry factor is given by

$$\frac{1}{2}(n'^{\uparrow\uparrow} + n'^{\uparrow\downarrow}) = \frac{N}{6\varepsilon_0}\alpha_{\alpha\alpha}(g) \tag{41}$$

which relates to the intensity of the OPA band.[33] Similar dissymmetry (or asymmetry) factors are defined for MCD and ECD

$$g_{\mathrm{ECD}} = \frac{2(n'^L - n'^R)}{(n'^L + n'^R)} = -\frac{2G'_{\alpha\alpha}(g)}{c_0 \cdot \alpha_{\alpha\alpha}(g)} \tag{42}$$

$$g_{\mathrm{MCD}}(B) = \frac{2[n'^L(B) - n'^L(-B)]}{[n'^L(B) + n'^L(-B)]} = -\frac{1}{2}\frac{B_z\varepsilon_{\alpha\beta\lambda}\alpha'^{(m)}_{\alpha\beta\lambda}}{\alpha_{\alpha\alpha}(g)} \tag{43}$$

The above expressions are used to evaluate the empirical relation $g_{\mathrm{MChD}} = g_{\mathrm{MCD}} \cdot g_{\mathrm{ECD}}$.[33]

2.1 Connection to (damped) response functions

The molecular quantity that yields the OPA spectrum is the imaginary component of the damped electric-dipole–electric dipole linear response function[26]

$$\alpha_{\alpha\beta}(g) = -\mathrm{Im}\langle\langle\mu_\alpha;\mu_\beta\rangle\rangle^{\gamma}_{\omega} \tag{44}$$

where μ_α indicates a cartesian component of the electric dipole operator, γ is the damping factor and ω is the damped (complex) frequency.

For ORD and ECD, the imaginary and real components of the damped magnetic dipole–electric dipole linear response function propagator are required, respectively[32,34]

$$G'_{\alpha\beta}(f) = \mathrm{Im}\langle\langle\mu_\alpha;m_\beta\rangle\rangle^{\gamma}_{\omega} \tag{45}$$

$$G'_{\alpha\beta}(g) = \mathrm{Re}\langle\langle\mu_\alpha;m_\beta\rangle\rangle^{\gamma}_{\omega} \tag{46}$$

where m_α is the magnetic dipole moment operator component.

For MOR and MCD, the relevant complex propagator is the quadratic response function involving two electric and one magnetic dipole operators[21,22]

$$\alpha'^{(m)}_{\alpha\beta\lambda}(f) = \mathrm{Im}\langle\langle\mu_\alpha;\mu_\beta,m_\lambda\rangle\rangle^{\gamma}_{\omega;0} \tag{47}$$

$$\alpha'^{(m)}_{\alpha\beta\lambda}(g) = -\mathrm{Re}\langle\langle\mu_\alpha;\mu_\beta,m_\lambda\rangle\rangle^{\gamma}_{\omega;0} \tag{48}$$

Generalizing the results of Ref. 24, for MChB, the molecular tensors $A'^{(m)}_{\alpha,\beta\rho,\lambda}(f)$ and $G^{(m)}_{\alpha\beta,\lambda}(f)$ in Eq. 15 correspond to the quadratic response functions

$$G^{(m)}_{\alpha\beta,\lambda}(-\omega;\omega,0)(f) = \quad \mathrm{Re}\langle\langle\mu_\alpha;m_\beta,m_\lambda\rangle\rangle^{\gamma}_{\omega,0} \tag{49}$$

$$A'^{(m)}_{\alpha,\beta\rho,\lambda}(-\omega;\omega,0)(f) = -\mathrm{Im}\langle\langle\mu_\alpha;\Theta_{\beta\rho},m_\lambda\rangle\rangle^{\gamma}_{\omega,0} \tag{50}$$

where $(\Theta_{\beta\rho})$ is the traceless quadrupole moment operator component. The fact that the equations above involve the electric dipole moment, the magnetic dipole moment and the traceless quadrupole moment operators raises the issue of origin invariance, which has been discussed in detail by Coriani and coworkers.[24] We refer to that source for further details on the calculation of magneto-chiral birefringence in non-absorbing regions of the sample.

When the frequency of the incident light approaches the absorbing region of the sample, the dichroism (MChD) emerges. Similar to what we did in the case of the magnetic circular dichroism,[21,22] we consider the absorptive counterparts of the quadratic

response functions describing the MChB, that is

$$G^{(m)}_{\alpha\beta,\lambda}(-\omega;\omega,0)(g) = \quad \mathrm{Im}\langle\langle \mu_\alpha; m_\beta, m_\lambda \rangle\rangle^{\gamma}_{\omega,0} \tag{51}$$

$$A'^{(m)}_{\alpha,\beta\rho,\lambda}(-\omega;\omega,0)(g) = -\mathrm{Re}\langle\langle \mu_\alpha; \Theta_{\beta\rho}, m_\lambda \rangle\rangle^{\gamma}_{\omega,0} \, . \tag{52}$$

3 Computational details

To start the investigation we chose the R-methyloxirane molecule as the smallest organic chiral system. Next, in order to stay in the context of biologically relevant species, we investigated a chiral proteinogenic aminoacid, L-alanine.

The calculations on R-methyloxirane were performed on the optimized structure of the (R) enantiomer taken from Ref. 24, where it has been obtained at the MP2/cc-pVTZ level of theory. For natural amino-acid L-alanine, we considered the equilibrium structures of the two lowest lying gas-phase conformers Ala-I and Ala-IIA fully optimized at the coupled-cluster [CCSD(T)/cc-pVTZ] level of theory by Jaeger et al.[35] The authors of Ref. 35 computed a relative energy between these two conformations of 2.11 kJ mol^{-1}, corresponding to Boltzmann weights of ≈0.7 and ≈0.3 for Ala-I and Ala-IIA, respectively. The same authors discuss a third conformer (labelled Ala-IIB) very close in energy to Ala-IIA and which they claimed as still unobserved when the paper was published. We did not include this conformer in our analysis. OPA, ECD, MCD and MOR as well as MChB and MChD spectra were computed both at the Hartree–Fock and at the TD-DFT level (B3LYP and CAMB3LYP functionals) in the (multiply-) augmented correlation consistent basis sets aug-cc-pVDZ, d-aug-cc-pVDZ, t-aug-cc-pVDZ. The convergence threshold of the response calculations was set to 10^{-5}.

In the CPP calculations, we used the empirical linewidth γ equal to 1000 cm^{-1} (0.00456 a.u.) and the step between successive frequencies in the transition region equal to 0.0025 a.u. Obviously, the choice of γ affects the calculated spectra, a larger value yielding broader spectral features with lower peak intensities. As we here deal with pure electronic structure calculations where various factors (such as vibronic couplings) affecting the experimental linewidths are not considered, the value of γ can be empirically adjusted to approximately match the observed spectra. So far there exist no experimental spectra for MChD for the chosen compounds, and we rely in our selection of γ in previous application of the CPP approach for MCD in systems of composition comparable to the present ones.[36,37]

The code to evaluate the MChD and MChB properties was implemented within the DALTON program.[38,39] The plots, obtained by spline fitting the computed observables, were done using the Python Scipy[40] and Matplotlib[41] libraries. The code was first tested against the MChB results obtained in Ref. 24 and it was found that the values obtained therein could be reproduced, in particular, the values of $B(A')$ and $B(G)$ for H_2O_2 and R-methyloxirane.

4 Results and discussion

As mentioned above, we have computed the dispersion and absorption spectra both at (TD)-Hartree–Fock and (TD-)DFT levels, the latter with two different functionals, and three basis sets, aug-cc-pVDZ, d-aug-cc-pVDZ and t-aug-cc-pVDZ. Spectra were simulated in the wavelength region including the lowest ten electronic excitations. The full set of results is collected in the Supplementary Information file, and we refrain in the following from a very detailed discussion, limiting ourselves to summarizing here the main points. The results reported and discussed in the following are those obtained in the largest (t-aug-cc-pVDZ) basis set.

For R-methyloxirane all three basis sets yield, for each individual electronic structure model, rather similar spectral profiles, the differences mainly emerging at higher frequencies (lower wavelengths) consistent with the increasing number of excited states when approaching the ionization limit.

Table 1 collects the excitation energies, the OPA oscillator strengths and the ECD rotational strengths of the first ten excitations.

Much more pronounced are the differences, in the same basis sets, between Hartree–Fock and DFT results, and, to a lower extent, between the two sets of DFT results. As commonly seen, Hartree–Fock spectra are shifted towards lower wavelengths (first excitation at 8.83 eV in the t-aug-cc-pVDZ basis), followed by the CAMB3LYP (first bright excitation at 7.01 eV) and then by the B3LYP (6.44 eV) ones. Note that the first ionization limit has been estimated by Koopmans' theorem at 11.8 eV for Hartree–Fock, at 9.26 eV for CAMB3LYP and 7.43 eV for B3LYP.

Despite the shift in the spectra and the underlying different composition of the bands in terms of individual excited states, both DFT functionals show qualitatively similar band features in the CPP spectra, see upper panels of Fig. 1.

The ECD spectrum has a $+/-$ band structure in both cases in correspondence to the first five excitations. The MCD spectrum exhibits a weak negative peak around the first excitation in the CAMB3LYP case, not evident in the B3LYP spectrum, otherwise both functionals yield a positive band in the region around the second to fourth excitation. The MChD spectra have a $-/+$ pattern for both functionals. Remarkably all three dichroisms show different sign patters, indicating that three effects yield complementary information.

Inspection of the figures also shows that the different spectroscopic effects have very different intensities (yet the two functionals give comparable intensities). The MCD signal is about one order of magnitude weaker (per unit of magnetic field) of the ECD one. The MChD signal is two to three orders of magnitude weaker than the MCD one.

The dispersion curves, see Fig. 1 (lower panels), also show some qualitatively similar features for the two functionals, and give an indication of the origin of the resonances in the MCD and MChD CPP spectra, as they correspond to inflection points on the dispersion profiles.

A detailed investigation of pure and cascaded magneto-chiral dichroism has led Rikken and Raupach[33] to the conclusion that in diamagnetic media, between the magnitude of the anisotropy factor for the pure magneto-chiral effect and that for natural and magnetic circular dichroism, the following relation should hold approximately:

$$|g_{\mathrm{MChD}}| \approx |g_{\mathrm{ECD}}||g_{\mathrm{MCD}}| \tag{53}$$

Table 1 Excitation energies, oscillator strengths (f) and rotational strengths (R) for the first 10 excitations of R-methyloxirane. Hartree–Fock and TD-DFT results in the t-aug-cc-pVDZ basis set.

	Hartree–Fock				CAMB3LYP				B3LYP			
No.	ω_i, eV	λ, nm	f	R	ω_i, eV	λ, nm	f	R	ω_i, eV	λ, nm	f	R
1	8.831	140.4	0.0026	−1.009	7.101	174.6	0.0075	−14.047	6.442	192.5	0.0092	−16.326
2	8.980	138.1	0.0068	4.706	7.365	168.3	0.0169	−8.042	6.836	181.4	0.0068	7.493
3	9.214	134.6	0.0457	−19.796	7.515	165.0	0.0134	8.717	6.866	180.6	0.0221	−2.007
4	9.265	133.8	0.0326	−10.746	7.671	161.6	0.0160	6.089	6.899	179.7	0.0040	5.471
5	9.366	132.4	0.0198	−4.041	7.851	157.9	0.0053	9.508	7.214	171.9	0.0005	−1.080
6	9.514	130.3	0.0130	−12.327	8.244	150.4	0.0090	−9.597	7.273	170.5	0.0007	0.616
7	9.648	128.5	0.0075	10.261	8.279	149.8	0.0147	9.733	7.280	170.3	0.0012	−0.250
8	9.870	125.6	0.0347	6.773	8.309	149.2	0.0260	−10.258	7.284	170.2	0.0009	0.911
9	9.997	124.0	0.0030	−2.728	8.349	148.5	0.0042	0.74	7.302	169.8	0.0056	6.634
10	10.160	122.0	0.0305	7.693	8.373	148.1	0.0103	−5.869	7.313	169.5	0.0001	0.243

For R-methyloxirane, the dissymmetry factors of ECD, MCD and MChD, together with their absolute values and the product of the ECD and MCD factors, are plotted in Fig. 2. The comparison shows that the curves yielded by the approximate relation above are rather different from those computed directly from the simulated MChD and OPA results, yet the order of magnitude is roughly the same. In the specific case the factor obtained from the ECD and MCD product is lower that the one computed directly for MChD.

Turning our attention to the two conformers of L-alanine, see Figs. 3 and 4 and ESI file, we note that, like in R-methyloxirane, the basis set effects on the spectra are contained, despite significant differences on the underlying composition of the spectral bands, as also appreciated from the results tabulated in Tables 2 and 3.

For Ala-I, a remarkable difference between B3LYP and CAMB3LYP is observed in the intermediate region of the ECD spectrum, which can be attributed to the different rotational strengths for the second and third excited states. The MCD spectra, on the other hand, are qualitatively similar in terms of band structure (+/−/+). An interesting feature in comparing the MCD and MChD spectra is the fact that no MChD band emerges around the second excited state, whereas it clearly does so in the MCD spectrum. As for R-methyloxirane, the predicted MChD intensities are roughly the same for both functionals, and significantly smaller than the MCD (and ECD) ones.

In Ala-IIA the sign pattern of the ECD bands corresponding to the lowest excited states is similar for the two functionals. The MCD signal is almost quenched in correspondence of the two first excited states (at least in the given ordinate scale), whereas a positive band emerges for the first excited state in the MChD spectrum. The larger separation between the first and second excited state probably accounts for the appearance of a weak band in the CAM spectrum in correspondence to the second excited state. For the higher states, the MCD and MChD signals have the same sign pattern, yet with a different composition in terms of contributions from the excited states underlying the various bands. Once again, the spectral intensities are comparable for the two functionals.

The dispersion profiles for OR, MOR and MChB have also been included in Figs. 3 and 4.

The two conformers have rather different spectra and dispersion profiles. The curves have been combined according to their Boltzmann weights and are shown in Fig. 5. The curves corresponding to the Ala-I and Ala-IIA conformers were included in the total spectrum with the factors of 0.7 and 0.3, respectively.

The corresponding dissymmetry factor curves are shown in Fig. 6.

5 Conclusions

A protocol for the calculation of magneto-chiral dichroism and magneto-chiral birefringence has been proposed and implemented within the complex polarization propagator formalism of Hartree–Fock and density functional response theory. Pilot results have been presented for R-methyloxirane and L-alanine. Despite the differences in the fine spectral details, both B3LYP and CAMB3LYP yield similar results (in terms of intensity) for the MChD, which is computed two to three orders of magnitude smaller than the corresponding MCD signal. The MChD dissymmetry factor curves are different from the product of the dissymmetry factors for MCD and ECD, but roughly of the same order of magnitude.

In a previous experiment on chromium tris-oxalate[42] a resolution of g of a few times 10^{-6} T^{-1} had been reached. The computational predictions are at the limit of the current experimental resolution, obtained in the visible wavelength range, and should stimulate the development of a similar resolution in the UV and deep UV, in view of the ongoing discussion on the role of magneto chiral dichroism in the homochirality of life. The rational search for organic molecules of biological relevance with a detectable magneto-chiral dichroism has just begun.

Appendix: More definitions and unit conversions

In terms of specific observables, rotations and ellipticities become, for NOA

$$[\alpha] \approx -\frac{\omega N_a}{3\varepsilon_0 c_0^2 M} G'_{\alpha\alpha}(f) \tag{54}$$

$$[\psi] \approx -\frac{\omega N_a}{3\varepsilon_0 c_0^2 M} G'_{\alpha\alpha}(g) \tag{55}$$

where M is the molar mass. The specific rotation (ellipticity) is obtained in the commonly used units of deg × cm^3 × dm^{-1} ×

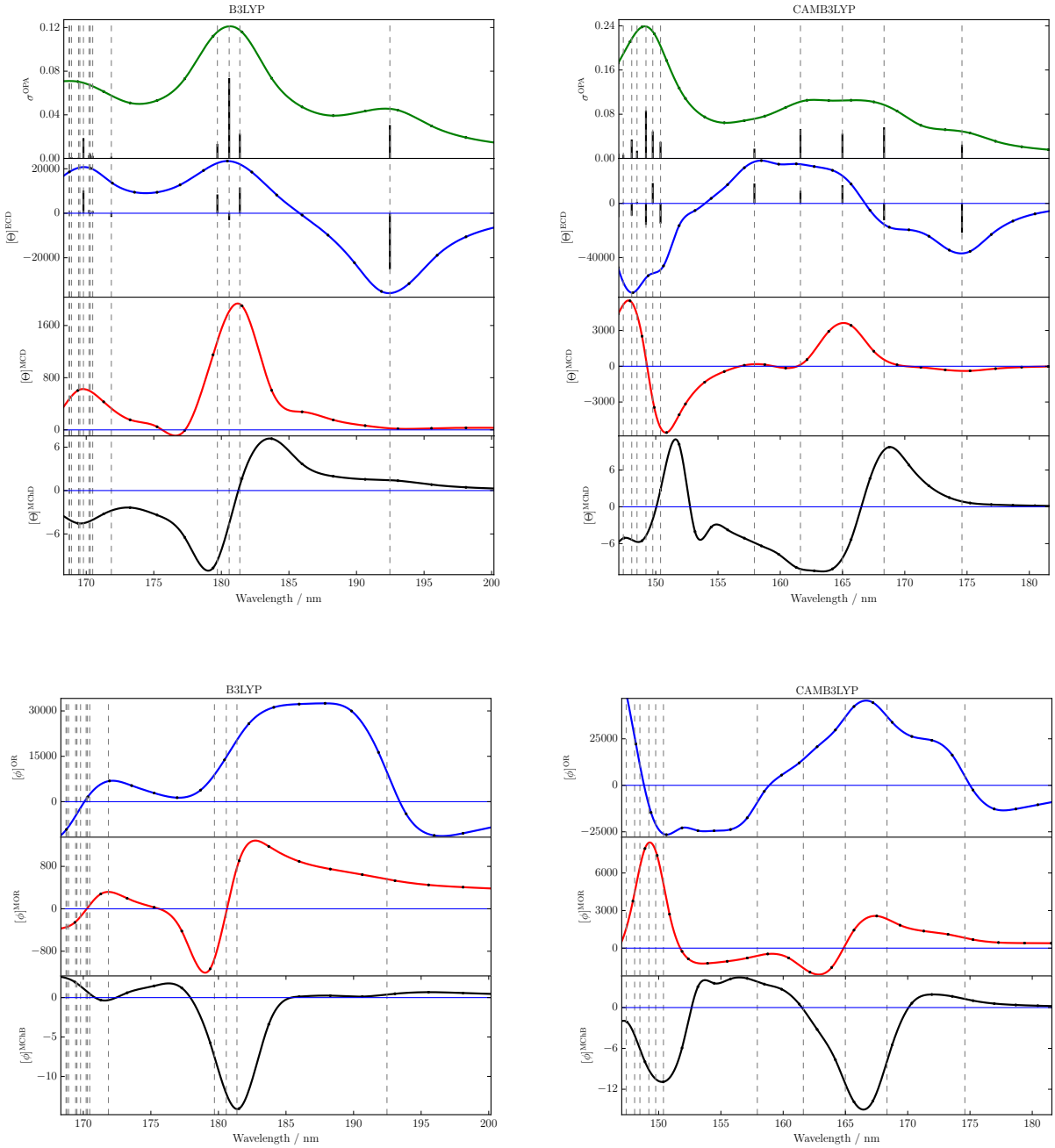

Fig. 1 R-methyloxirane. Upper panels: One Photon Absorption (OPA) cross sections, Electronic Circular Dichroism (ECD), Magnetic Circular Dichroism (MCD) and Magneto-chiral Dichroism (MChD) calculated at the B3LYP/t-aug-cc-pVDZ (left) and CAMB3LYP/t-aug-cc-pVDZ (right) levels. Lower panels: Natural Optical Rotatory (OR), Magnetic Optical Rotation (MOR) and Magneto-chiral Birefringence (MChB) dispersions calculated at the B3LYP/t-aug-cc-pVDZ (left) and CAMB3LYP/t-aug-cc-pVDZ (right) levels. Absorption cross sections are reported in atomic units. All other quantities are given in deg$\times$dm$^3\times$cm$^{-1}\times$mol^{-1}. MCD, MChD, MOR and MChB spectra were computed at 1 T of magnetic field intensity.

Table 2 Excitation energies, oscillator strengths (f) and rotational strengths (R) for the first 10 excitations of Ala-I. Hartree–Fock and TD-DFT results in the t-aug-cc-pVDZ basis set. Ionisation potentials according to Koopmans' theorem: B3LYP = 7.12 eV; CAMB3LYP=8.92 eV; SCF=11.24 eV

	Hartree–Fock				CAMB3LYP				B3LYP			
No.	ω_i, eV	λ, nm	f	R	ω_i, eV	λ, nm	f	R	ω_i, eV	λ, nm	f	R
1	6.625	187.1	0.0016	8.218	5.806	213.5	0.0012	7.65	5.591	221.8	0.0024	7.249
2	7.760	159.8	0.0214	−2.045	6.363	194.9	0.0123	−1.519	5.870	211.2	0.0046	−7.145
3	8.654	143.3	0.0105	1.091	6.664	186.1	0.0025	1.518	5.972	207.6	0.0012	7.463
4	8.875	139.7	0.0336	12.43	7.070	175.4	0.0763	−13.15	6.323	196.1	0.0605	−3.580
5	8.918	139.0	0.0622	−38.31	7.171	172.9	0.0076	−2.206	6.527	190.0	0.0018	−0.928
6	9.324	133.0	0.0273	2.183	7.394	167.7	0.0062	−0.637	6.644	186.6	0.0106	3.214
7	9.404	131.8	0.0353	9.016	7.524	164.8	0.0077	1.751	6.694	185.2	0.0162	−9.533
8	9.525	130.2	0.0766	−4.452	7.856	157.8	0.0073	−0.374	6.900	179.7	0.0003	−0.481
9	9.546	129.9	0.0004	−0.775	7.951	155.9	0.0053	5.397	6.956	178.2	0.0006	0.109
10	9.641	128.6	0.0053	−1.803	7.979	155.4	0.0016	0.294	6.976	177.7	0.0001	−0.045

Table 3 Excitation energies, oscillator strengths (f) and rotational strengths R for the first 10 excitations of Ala-IIA. Hartree–Fock and TD-DFT results in the t-aug-cc-pVDZ basis set. Ionisation potentials according to Koopmanns theorem: B3LYP = 7.27 eV; CAMB3LYP= 9.08 eV; SCF=11.54 eV

	Hartree–Fock				CAMB3LYP				B3LYP			
No.	ω_i, eV	λ, nm	f	R	ω_i, eV	λ, nm	f	R	ω_i, eV	λ, nm	f	R
1	6.4805	191.3	0.0015	1.759	5.664	218.9	0.0010	3.967	5.536	224.0	0.0014	11.68
2	7.8523	157.9	0.0166	1.634	6.420	193.1	0.0098	−4.790	5.759	215.3	0.0106	−12.91
3	8.8477	140.1	0.0412	−9.635	7.124	174.0	0.0402	4.835	6.559	189.0	0.0008	−2.827
4	9.0465	137.0	0.0055	12.44	7.374	168.1	0.0015	−1.924	6.602	187.8	0.0296	2.747
5	9.1889	134.9	0.0614	−16.92	7.505	165.2	0.0100	−11.31	6.704	184.9	0.0014	−2.127
6	9.2661	133.8	0.1258	8.618	7.593	163.3	0.0126	−9.311	6.772	183.1	0.0128	−9.692
7	9.5483	129.8	0.0096	2.867	7.817	158.6	0.0093	−5.362	7.010	176.9	0.0009	−0.422
8	9.6668	128.2	0.0202	−16.92	7.973	155.5	0.0040	−2.759	7.069	175.4	0.0074	−6.236
9	9.6709	128.2	0.0004	2.49	8.053	154.0	0.0003	−0.604	7.110	174.4	0.0003	−0.432
10	9.8265	126.2	0.0085	5.183	8.106	153.0	0.0006	0.964	7.124	174.0	0.0001	−0.069

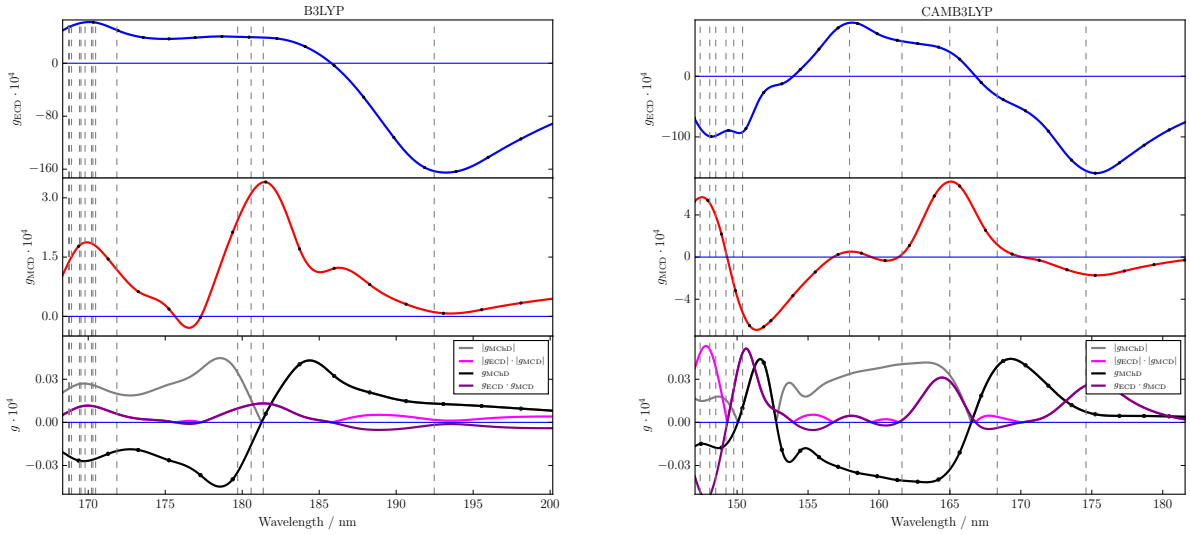

Fig. 2 R-methyloxirane. The g_{ECD}, g_{MCD} and g_{MChD} dissimmetry factors, calculated at the B3LYP/t-aug-cc-pVDZ (left) and CAMB3LYP/t-aug-cc-pVDZ (right) levels. Note that the MCD and MChD dissymmetry factors are given for 1 T of magnetic field intensity.

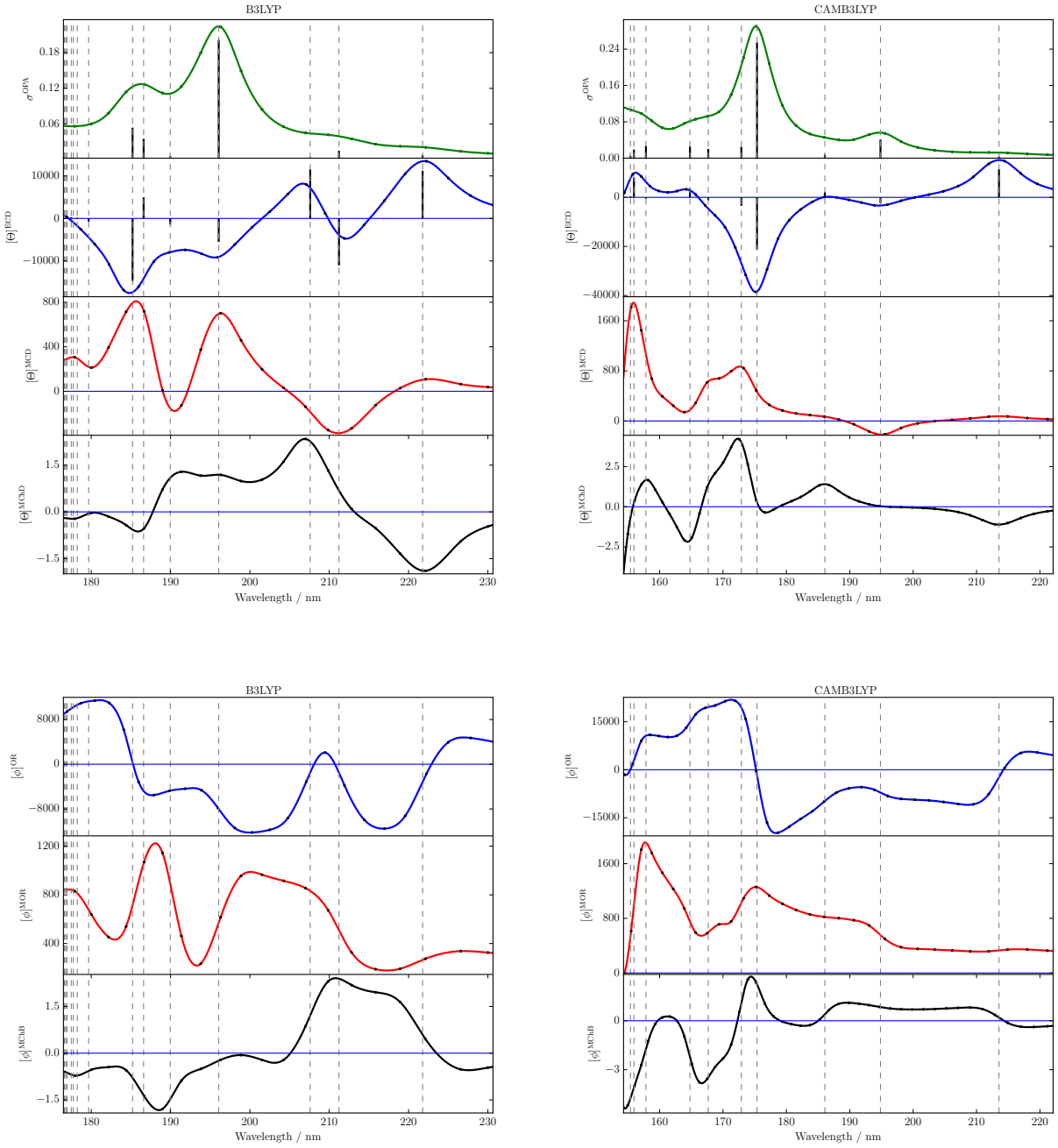

Fig. 3 L-Alanine, conformer I. Upper panels: One Photon Absorption (OPA) cross sections, Electronic Circular Dichroism (ECD), Magnetic Circular Dichroism (MCD) and Magneto-chiral Dichroism (MChD), calculated at the B3LYP/t-aug-cc-pVDZ (left) and CAMB3LYP/t-aug-cc-pVDZ (right) levels.Lower panels: Natural Optical Rotatory (OR), Magnetic Optical Rotation (MOR) and Magneto-chiral Birefringence (MChB) dispersions, calculated at B3LYP/t-aug-cc-pVDZ (left) and CAMB3LYP/t-aug-cc-pVDZ (right) levels. Absorption cross sections are reported in atomic units. All other quantities are given in deg$\times$dm$^3\times$cm$^{-1}\times$mol^{-1}. MCD, MChD, MOR and MChB spectra were computed at 1 T of magnetic field intensity.

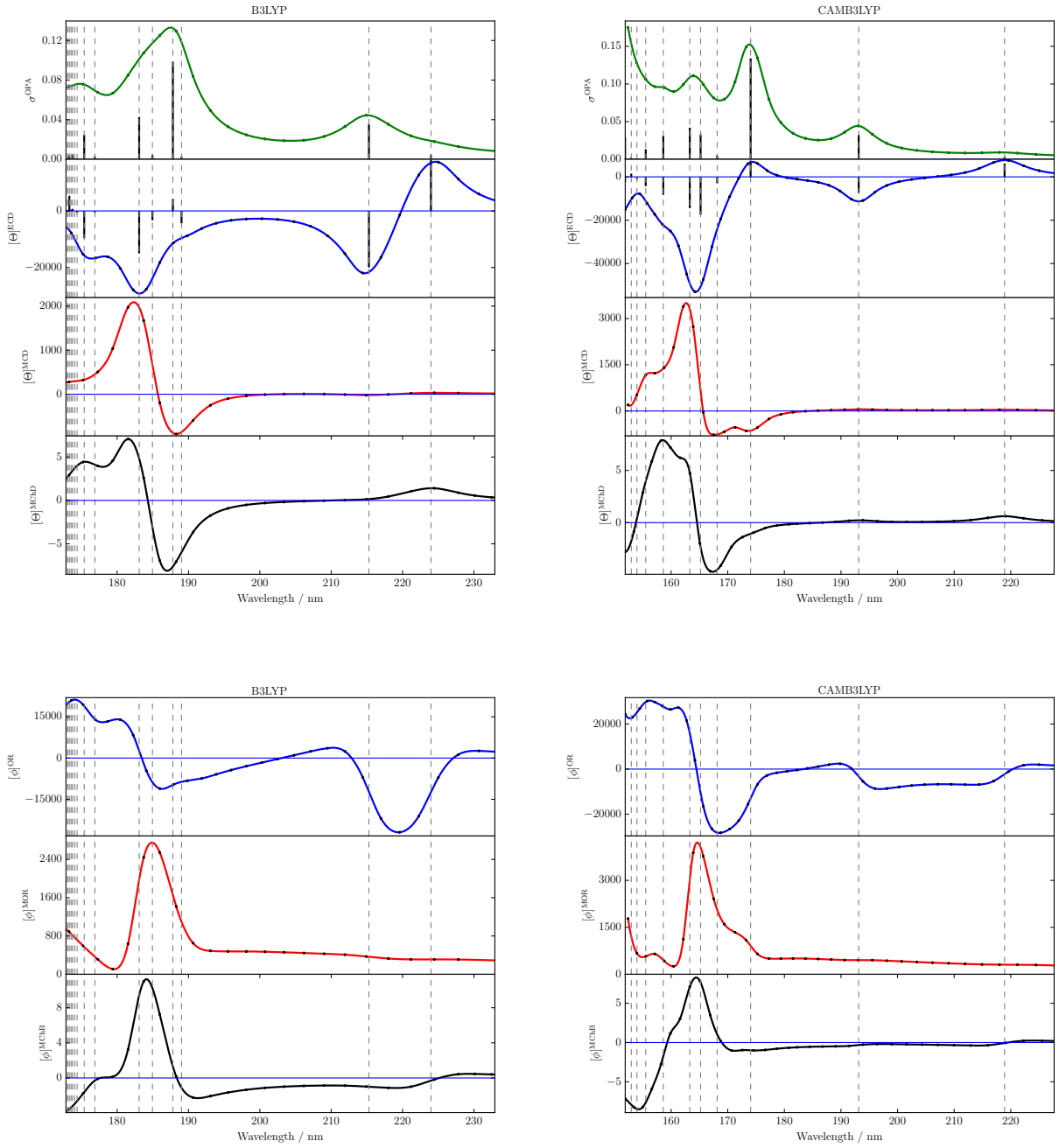

Fig. 4 L-Alanine, conformer IIA. Upper panels: One Photon Absorption (OPA) cross section, Electronic Circular Dichroism (ECD), Magnetic Circular Dichroism (MCD) and Magneto-chiral Dichroism (MChD), calculated at B3LYP/t-aug-cc-pVDZ (left) and CAMB3LYP/t-aug-cc-pVDZ (right) levels of theory. Lower panels: Natural Optical Rotatory (OR), Magnetic Optical Rotation (MOR) and Magneto-chiral Birefringence (MChB) dispersions, calculated at B3LYP/t-aug-cc-pVDZ (left) and CAMB3LYP/t-aug-cc-pVDZ (right) levels of theory. Absorption cross sections are reported in atomic units. OAll other quantities are given in deg$\times$dm$^3\times$cm$^{-1}\times$mol^{-1}. MCD, MChD, MOR and MChB spectra were computed at 1 T of magnetic field intensity.

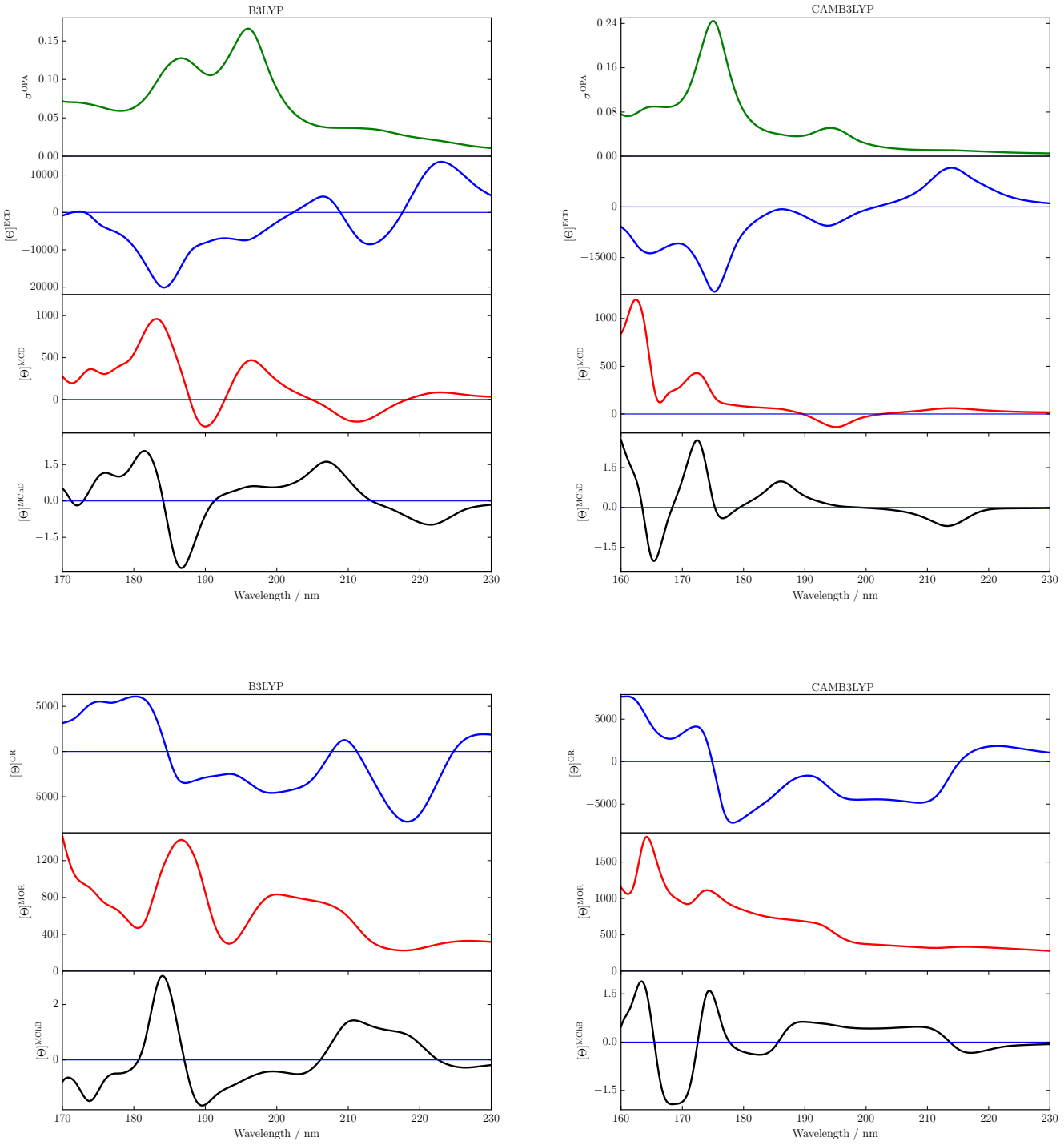

Fig. 5 L-Alanine. Boltzmann averages. Upper panels: One Photon Absorption (OPA) cross sections, Electronic Circular Dichroism (ECD), Magnetic Circular Dichroism (MCD) and Magneto-chiral Dichroism (MChD), calculated at the B3LYP/t-aug-cc-pVDZ (left) and CAMB3LYP/t-aug-cc-pVDZ (right) levels. Lower panels: Natural Optical Rotatory (OR), Magnetic Optical Rotation (MOR) and Magneto-chiral Birefringence (MChB) dispersions, calculated at B3LYP/t-aug-cc-pVDZ (left) and CAMB3LYP/t-aug-cc-pVDZ (right) levels. Absorption cross sections are reported in atomic units. All other quantities are given in deg$\times$dm$^3\times$cm$^{-1}\times$mol^{-1}. MCD, MChD, MOR and MChB spectra were computed at 1 T of magnetic field intensity.

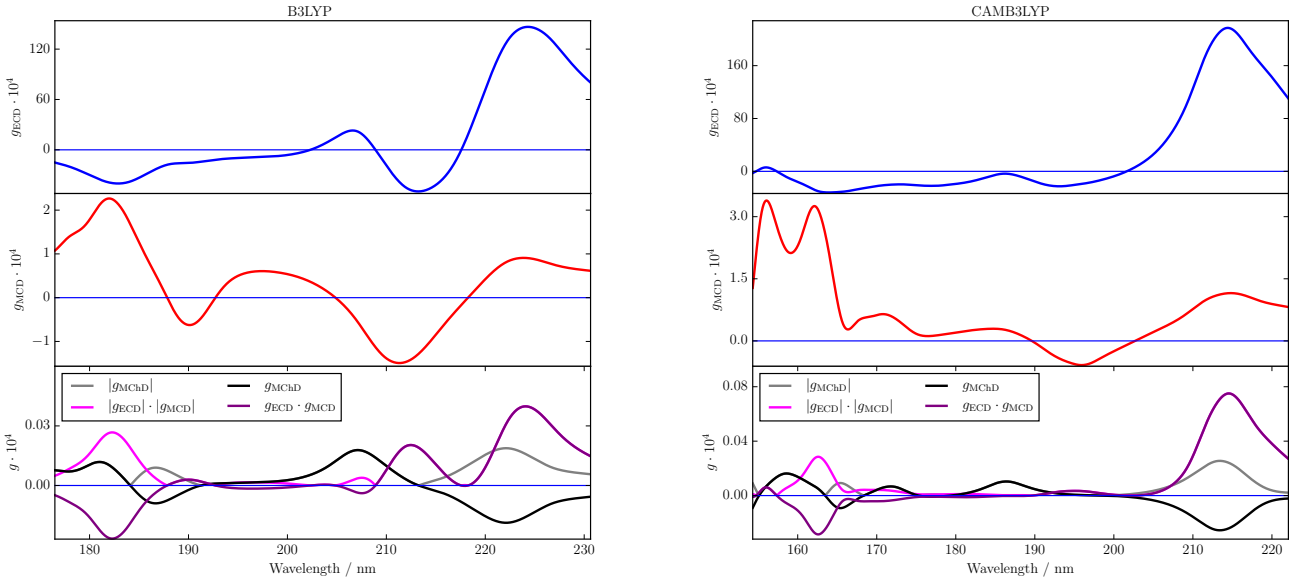

Fig. 6 Alanine. The g_{ECD}, g_{MCD} and g_{MChD} dissimmetry factors, calculated at the B3LYP/t-aug-cc-pVDZ (left) and CAMB3LYP/t-aug-cc-pVDZ (right) level of theory from the Boltzmann averaged spectra. Note that the MCD and MChD dissymmetry factors were computed at 1 T of magnetic field intensity.

gr^{-1} using the expressions

$$[\alpha][\mathrm{deg}\times\mathrm{cm}^3\times\mathrm{dm}^{-1}\times\mathrm{gr}^{-1}]\approx \tag{56}$$
$$-2.15524\times10^6\times\frac{\omega[\mathrm{au}]}{M[\mathrm{gr\ mol}^{-1}]}\times G'_{\alpha\alpha}(f)[\mathrm{au}]$$

$$[\psi][\mathrm{deg}\times\mathrm{cm}^3\times\mathrm{dm}^{-1}\times\mathrm{gr}^{-1}]\approx \tag{57}$$
$$-2.15524\times10^6\times\frac{\omega[\mathrm{au}]}{M[\mathrm{gr\ mol}^{-1}]}\times G'_{\alpha\alpha}(g)[\mathrm{au}]$$

For MOA

$$[\alpha]\approx-\frac{\omega N_a}{12\varepsilon_0 c_0 M}B_z\varepsilon_{\alpha\beta\gamma}\alpha'^{(m)}_{\alpha\beta\gamma}(f) \tag{58}$$

$$[\psi]\approx-\frac{\omega N_a}{12\varepsilon_0 c_0 M}B_z\varepsilon_{\alpha\beta\gamma}\alpha'^{(m)}_{\alpha\beta\gamma}(g) \tag{59}$$

$$[\alpha][\mathrm{deg}\times\mathrm{cm}^3\times\mathrm{dm}^{-1}\times\mathrm{gr}^{-1}]\approx \tag{60}$$
$$-3.14128\times10^2\times\frac{\omega[\mathrm{au}]}{M[\mathrm{gr\ mol}^{-1}]}\times B_z[\mathrm{T}]\times\varepsilon_{\alpha\beta\gamma}\times\alpha'^{(m)}_{\alpha\beta\gamma}(f)[\mathrm{au}]$$

$$[\psi][\mathrm{deg}\times\mathrm{cm}^3\times\mathrm{dm}^{-1}\times\mathrm{gr}^{-1}]\approx \tag{61}$$
$$-3.14128\times10^2\times\frac{\omega[\mathrm{au}]}{M[\mathrm{gr\ mol}^{-1}]}\times B_z[\mathrm{T}]\times\varepsilon_{\alpha\beta\gamma}\times\alpha'^{(m)}_{\alpha\beta\gamma}(g)[\mathrm{au}]$$

and for MChD and MChB

$$[\alpha]\approx-\frac{\omega N_a}{6\varepsilon_0 c_0^2 M}B_z\left\{B^{A'}(f)+B^G(f)\right\} \tag{62}$$

$$[\psi]\approx-\frac{\omega N_a}{6\varepsilon_0 c_0^2 M}B_z\left\{B^{A'}(g)+B^G(g)\right\} \tag{63}$$

$$[\alpha][\mathrm{deg}\times\mathrm{cm}^3\times\mathrm{dm}^{-1}\times\mathrm{gr}^{-1}]\approx \tag{64}$$
$$-4.58460\times\frac{\omega[\mathrm{au}]}{M[\mathrm{gr\ mol}^{-1}]}\times B_z[\mathrm{T}]\times\left\{B^{A'}(f)+B^G(f)\right\}[\mathrm{au}]$$

$$[\psi][\mathrm{deg}\times\mathrm{cm}^3\times\mathrm{dm}^{-1}\times\mathrm{gr}^{-1}]\approx \tag{65}$$
$$-4.58460\times\frac{\omega[\mathrm{au}]}{M[\mathrm{gr\ mol}^{-1}]}\times B_z[\mathrm{T}]\times\left\{B^{A'}(g)+B^G(g)\right\}[\mathrm{au}]$$

Here we also give a compilation of relevant conversion units:

- $\varepsilon_0 = 8.85419\times10^{-12}\ \mathrm{F\ m}^{-1} = 7.95775\times10^{-2}\ a_0 m_e e^2\hbar^{-2}$;
- $c_0 = 299\ 792\ 459\ \mathrm{m\ s}^{-1} = 1.37036\times10^2\ \hbar a_0^{-1} m_e^{-1}$;
- $N_a = 6.02214\times10^{23}\ \mathrm{mol}^{-1}$;
- $[\omega]\rightarrow \mathrm{s}^{-1} = 2.4188\times10^{-17}\hbar a_0^{-2} m_e^{-1}$;
- $[B_z]\rightarrow \mathrm{T} = 4.25438\times10^{-6}\hbar e^{-1} a_0^{-2}$;
- $[N]\rightarrow \mathrm{m}^{-3} = 1.48185\times10^{-31} a_0^3$;
- $[M]\rightarrow \mathrm{gr\ mol}^{-1} = 1.09777\times10^{27} m_e\ \mathrm{mol}^{-1}$;
- $[\alpha_{\alpha\beta}]\rightarrow \mathrm{C}^2\ \mathrm{m}^2\ \mathrm{J}^{-1} = 6.06510\times10^{40} e^2 a_0^4 m_e\hbar^{-2}$;
- $[G_{\alpha\beta}]\rightarrow \mathrm{C}^2\ \mathrm{m}^3\ \mathrm{J}^{-1}\ \mathrm{s}^{-1} = 2.77238\times10^{34}\hbar^{-1} a_0^3 e^2$;

- $[A_{\alpha,\beta\gamma}] \rightarrow \mathrm{C}^2\ \mathrm{m}^3\ \mathrm{J}^{-1} = 1.14614 \times 10^{51} \hbar^{-2} a_0^5 e^2 m_e$;
- $[\alpha'^{(m)}_{\alpha\beta\gamma}] \rightarrow \mathrm{C}^3\ \mathrm{m}^4\ \mathrm{s}^{-1}\ \mathrm{J}^{-2} = 1.42561 \times 10^{46} e^3 a_0^6 \hbar^{-3} m_e$;
- $[G^{(m)}_{\alpha\beta,\gamma}] \rightarrow \mathrm{C}^3\ \mathrm{m}^5\ \mathrm{J}^{-2}\ \mathrm{s}^{-2} = 6.51652 \times 10^{39} e^3 a_0^5 \hbar^{-2}$;
- $[A^{(m)}_{\alpha\beta\gamma\delta}] \rightarrow \mathrm{C}^3\ \mathrm{m}^5\ \mathrm{J}^{-2}\ \mathrm{s}^{-1} = 2.69402 \times 10^{56} e^3 a_0^7 m_e \hbar^{-3}$;

Acknowledgments

This research work was carried out with support from the University of Trieste (Grant CHIM02-Ricerca, J.C. and S.C.), the PRIN2009 funding scheme (Project No. 2009C28YBF_001, S.C.), the AIAS-COFUND Marie-Curie program (Grant Agreement No. 609033, S.C.), the COST-CMTS Action CM1002 COnvergent Distributed Environment for Computational Spectroscopy (CODECS), the Interdisciplinary Centre for Mathematical and Computational Modelling (ICM), University of Warsaw (Grant No. G56-20, J.C.). Computer time from CINECA-UniTS and the National Supercomputer Centre (NSC) in Linköping is also acknowledged.

References

1 L. D. Barron, *Molecular light scattering and optical activity*, Cambridge University Press, Cambridge, 2004.
2 G. H. Wagnière and A. Meyer, *Chem. Phys. Lett.*, 1982, **93**, 78–81.
3 G. H. Wagnière, *Chem. Phys. Lett.*, 1984, **110**, 546–551.
4 L. Barron and J. Vrbancich, *Mol. Phys.*, 1984, **51**, 715–730.
5 G. L. Rikken and E. Raupach, *Nature*, 1997, **390**, 493–494.
6 G. Wagnière, *Chem. Phys.*, 1999, **245**, 165–173.
7 G. L. Rikken and E. Raupach, *Nature*, 2000, **405**, 932–5.
8 G. H. Wagnière and G. L. Rikken, *Chem. Phys. Lett.*, 2009, **481**, 166–168.
9 G. H. Wagnière, *On Chirality and the Universal Asymmetry. Reflections on Image and Mirror Image*, Wiley-VCH, Zurich, 2007.
10 L. Barron, *Nature*, 2000, **405**, 895.
11 N. B. Baranova, Y. V. Bogdanov and B. Y. Zel'dovich, *Opt. Commun.*, 1977, **22**, 243–247.
12 G. H. Wagnière and A. Meier, *Experimentia*, 1983, **39**, 1090.
13 Y. Kitagawa, H. Segawa and K. Ishii, *Angew. Chem. Int. Ed.*, 2011, **50**, 9133.
14 Y. Kitagawa, T. Miyatake and K. Ishii, *Chem. Comm.*, 2012, **48**, 5091–3.
15 R. Sessoli, M.-E. Boulon, A. Caneschi, M. Mannini, L. Poggini, F. Wilhelm and A. Rogalev, *Nat. Phys.*, 2015, **11**, 69–74.
16 A. D. Buckingham and P. J. Stephens, *Ann. Rev. Phys. Chem.*, 1966, 399–432.
17 W. R. Mason, *A Practical guide to Magnetic Circular Dichroism Spectroscopy*, Wiley, New York, 2007.
18 T. Kjærgaard, S. Coriani and K. Ruud, *WIREs: Comput. Mol. Sci.*, 2012, **2**, 443–455.
19 S. Coriani, P. Jørgensen, A. Rizzo, K. Ruud and J. Olsen, *Chem. Phys. Lett.*, 1999, **300**, 61–68.
20 S. Coriani, C. Hättig, P. Jørgensen and T. Helgaker, *J. Chem. Phys.*, 2000, **113**, 3561.
21 H. Solheim, K. Ruud, S. Coriani and P. Norman, *J. Chem. Phys.*, 2008, **128**, 094103.
22 T. Kjærgaard, K. Kristensen, J. Kauczor, P. Jørgensen, S. Coriani and A. Thorvaldsen, *J. Chem. Phys.*, 2011, **135**, 024112.
23 T. Fahleson, J. Kauczor, P. Norman and S. Coriani, *Mol. Phys.*, 2013, **111**, 1401–1404.
24 S. Coriani, M. Pecul, A. Rizzo, P. Jørgensen and M. Jaszunski, *J. Chem. Phys.*, 2002, **117**, 6417.
25 B. Jansík, A. Rizzo, L. Frediani, K. Ruud and S. Coriani, *J. Chem. Phys.*, 2006, **125**, 234105.
26 P. Norman, D. Bishop, H. Jensen and J. Oddershede, *J. Chem. Phys.*, 2001, **115**, 10323.
27 P. Norman, D. Bishop, H. Jensen and J. Oddershede, *J. Chem. Phys.*, 2005, **123**, 194103.
28 K. Kristensen, J. Kauczor, T. Kjærgaard and P. Jørgensen, *J. Chem. Phys.*, 2009, **131**, 044112.
29 P. Norman, *Phys. Chem. Chem. Phys.*, 2011, **13**, 20519.
30 J. Kauczor, P. Jørgensen and P. Norman, *J. Chem. Theory Comput.*, 2011, **7**, 1610.
31 A. D. Buckingham, *Adv. Chem. Phys.*, 1967, **12**, 107.
32 A. Jiemchooroj and P. Norman, *J. Chem. Phys.*, 2007, **126**, 134102.
33 G. L. Rikken and E. Raupach, *Phys. Rev. E*, 1998, **58**, 5081–5084.
34 P. Norman, K. Ruud and T. Helgaker, *J. Chem. Phys.*, 2004, **120**, 5027.
35 H. M. Jaeger, H. F. Schaefer III, J. Demaison, A. G. Császár and W. D. Allen, *J. Chem. Theory Comput.*, 2010, **6**, 3066–3078.
36 F. Santoro, R. Improta, T. Fahleson, J. Kauczor, P. Norman and S. Coriani, *J. Phys. Chem. Lett.*, 2014, **5**, 1806–1811.
37 T. Fahleson, J. Kauczor, P. Norman, F. Santoro, R. Improta and S. Coriani, *J. Phys. Chem. A*, 2015, **119**, 5476–5489.
38 K. Aidas, C. Angeli, K. L. Bak, V. Bakken, R. Bast, L. Boman, O. Christiansen, R. Cimiraglia, S. Coriani, P. Dahle, E. K. Dalskov, U. Ekström, T. Enevoldsen, J. J. Eriksen, P. Ettenhuber, B. Fernández, L. Ferrighi, H. Fliegl, L. Frediani, K. Hald, A. Halkier, C. Hättig, H. Heiberg, T. Helgaker, A. C. Hennum, H. Hettema, E. Hjertenæs, S. Høst, I.-M. Høyvik, M. F. Iozzi, B. Jansìk, H. J. A. Jensen, D. Jonsson, P. Jørgensen, J. Kauczor, S. Kirpekar, T. Kjærgaard, W. Klopper, S. Knecht, R. Kobayashi, H. Koch, J. Kongsted, A. Krapp, K. Kristensen, A. Ligabue, O. B. Lutnæs, J. I. Melo, K. V. Mikkelsen, R. H. Myhre, C. Neiss, C. B. Nielsen, P. Norman, J. Olsen, J. M. H. Olsen, A. Osted, M. J. Packer, F. Pawlowski, T. B. Pedersen, P. F. Provasi, S. Reine, Z. Rinkevicius, T. A. Ruden, K. Ruud, V. V. Rybkin, P. Sałek, C. C. M. Samson, A. S. de Merás, T. Saue, S. P. A. Sauer, B. Schimmelpfennig, K. Sneskov, A. H. Steindal, K. O. Sylvester-Hvid, P. R. Taylor, A. M. Teale, E. I. Tellgren, D. P. Tew, A. J. Thorvaldsen, L. Thøgersen, O. Vahtras, M. A. Watson, D. J. D. Wilson, M. Ziolkowski and H. Ågren, *WIREs Comput. Mol. Sci.*, 2014, **4**, 269–284.
39 DALTON, *a molecular electronic structure program, Release Dalton2015*, 2015, See http://daltonprogram.org/.

40 E. Jones, T. Oliphant, P. Peterson *et al.*, *SciPy: Open source scientific tools for Python*, 2001, `http://www.scipy.org/`, [Online; accessed 2016-02-06].

41 J. D. Hunter, *Computing in Science & Engineering*, 2007, **9**, 90–95.

42 E. Raupach, G. Rikken, C. Train and B. Malezieux, *Chem. Phys.*, 2000, **261**, 373–380.